Accepted for publication in ApJ
Preprint typeset using LaTeX style emulateapj v. 6/22/04

DIRECT MEASUREMENTS OF THE STELLAR CONTINUA AND BALMER/4000 Å BREAKS OF RED $Z > 2$ GALAXIES: REDSHIFTS AND IMPROVED CONSTRAINTS ON STELLAR POPULATIONS[1,2,3]

Mariska Kriek[4], Pieter G. van Dokkum[5], Marijn Franx[4], Natascha M. Förster Schreiber[6], Eric Gawiser[5], Garth D. Illingworth[7], Ivo Labbé[8,9], Danilo Marchesini[5], Ryan Quadri[5], Hans-Walter Rix[10], Gregory Rudnick[11,12], Sune Toft[5], Paul van der Werf[4], and Stijn Wuyts[4]

Accepted for publication in ApJ

ABSTRACT

We use near-infrared (NIR) spectroscopy obtained with GNIRS on Gemini, NIRSPEC on KECK, and ISAAC on the VLT to study the rest-frame optical continua of three 'Distant Red Galaxies' (having $J_s - K_s > 2.3$) at $z > 2$. All three galaxy spectra show the Balmer/4000 Å break in the rest-frame optical. The spectra allow us to determine spectroscopic redshifts from the continuum with an estimated accuracy $\Delta z/(1+z) \sim 0.001 - 0.04$. These redshifts agree well with the emission line redshifts for the 2 galaxies with Hα emission. This technique is particularly important for galaxies that are faint in the rest-frame UV, as they are underrepresented in high redshift samples selected in optical surveys and are too faint for optical spectroscopy. Furthermore, we use the break, continuum shape, and equivalent width of Hα together with evolutionary synthesis models to constrain the age, star formation timescale, dust content, stellar mass and star formation rate of the galaxies. Inclusion of the NIR spectra in the stellar population fits greatly reduces the range of possible solutions for stellar population properties. We find that the stellar populations differ greatly among the three galaxies, ranging from a young dusty starburst with a small break and strong emission lines to an evolved galaxy with a strong break and no detected line emission. The dusty starburst galaxy has an age of 0.3 Gyr and a stellar mass of 1 $\times 10^{11}$ $M_\odot$. The spectra of the two most evolved galaxies imply ages of 1.3-1.4 Gyr and stellar masses of 4×10^{11} $M_\odot$. The large breaks for the two most evolved galaxies indicate that active galactic nuclei (AGN) do not dominate the rest-frame optical continuum emission of these galaxies, while for the younger starburst a significant contribution from an AGN cannot be ruled out. The large range of properties seen in these galaxies strengthens our previous much more uncertain results from broadband photometry. Larger samples are required to determine the relative frequency of dusty starbursts and (nearly) passively evolving galaxies at $z \sim 2.5$.

Subject headings: galaxies: high redshift — galaxies: evolution — infrared: galaxies

1. INTRODUCTION

Recent studies have demonstrated that galaxies at $z > 2$ show a large range in their rest-frame optical colors. Deep near-infrared (NIR) imaging has allowed the identification of a new class of $z > 2$ galaxies, complementary to the Lyman break galaxies (LBGs, Steidel et al. 1996a,b) found in optical surveys. Franx et al. (2003) introduced the simple color criterion $J_s - K_s > 2.3$, to efficiently and successfully select red $z > 2$ galaxies (Distant Red Galaxies, or DRGs; Förster Schreiber et al. 2004; van Dokkum et al. 2004). The red colors can be caused by evolved stellar populations, dust, or a combination of both. It is difficult to assess the origin of the red colors from optical-to-NIR photometry alone (see Förster Schreiber et al. 2004). The extension of photometric studies to the rest-frame NIR wavelength regime helps: using IRAC on *Spitzer*, Labbé et al. (2005) distinguish the old from the dusty system much more reliably than was previously possible, and find that a significant part (30%) of the DRG sample is indeed best described by old and passively evolving stellar population models. This result is supported by the *Spitzer* 24 μm imaging presented by Webb et al. (2006), who find that 65% of the DRGs host dusty star-forming stellar populations. Similar findings have also been reported by Papovich et al. (2006) and Reddy et al. (2005) based on optical to mid-infrared photometry of the GOODS-South and North fields

Although our insight in the nature of $z > 2$ galaxies has significantly improved by the recent access to the rest-frame NIR and IR wavelength regime, broadband photo-

Electronic address: mariska@strw.leidenuniv.nl

[1] Based on observations obtained at the Gemini Observatory, which is operated by the Association of Universities for Research in Astronomy, Inc., under a cooperative agreement with the NSF on behalf of the Gemini partnership: the National Science Foundation (United States), the Particle Physics and Astronomy Research Council (United Kingdom), the National Research Council (Canada), CONICYT (Chile), the Australian Research Council (Australia), CNPq (Brazil) and CONICET (Argentina).

[2] Based on observations at the W.M. Keck Observatory, which is operated jointly by the California Institute of Technology and the University of California.

[3] Based on observations collected at the European Southern Observatory, Paranal, Chile

[4] Leiden Observatory, PO Box 9513, 2300 RA Leiden, The Netherlands

[5] Department of Astronomy, Yale University, P.O. Box 208101, New Haven, CT 06520-8101

[6] Max-Planck-Institut für extraterrestrische Physik, Giessenbachstrasse, Postfach 1312, D-85748 Garching, Germany

[7] UCO/Lick Observatory, University of California, Santa Cruz, CA 95064

[8] Carnegie Observatories, 813 Santa Barbara Street, Pasadena, CA 91101

[9] Carnegie Fellow

[10] Max-Planck-Institute für Astronomie, Königstuhl 17, Heidelberg, Germany

[11] National Optical Astronomy Observatory, 950 North Cherry Avenue, Tucson, AZ 85719

[12] Goldberg fellow

metric studies have their limitations. First, as spectral details get lost, the origin of the observed emission is uncertain. Emission lines may affect the broadband fluxes, and a possible contribution by an active galactic nucleus (AGN) is difficult to quantify. Second, the modeling results suffer from degeneracies between age, dust and the star formation history, especially when no spectroscopic redshift is available.

The large samples of confirmed high-redshift galaxies available today (e.g. Steidel et al. 2003; Vanzella et al. 2005) give the impression that obtaining spectroscopic redshifts is relatively easy. The most efficient and popular technique in obtaining redshifts for large samples of high redshift galaxies is multi-object spectroscopy at optical wavelengths. However, as about 75% of $2 < z < 3$ galaxies with $M > 10^{11}\mathrm{M}_{\odot}$ have $R > 25$ (van Dokkum et al. 2006), most are well beyond the limits of optical spectroscopy. Thus NIR spectroscopy is needed to obtain redshifts for these UV-faint galaxies.

For UV-faint passively evolving galaxies, which lack emission lines in their rest-frame optical, we are limited to the rest-frame optical stellar continuum to measure a redshift. The most easily detectable feature in the spectrum of evolved stars, and thus the best option to confirm redshifts of $z > 2$ evolved galaxies, is the Balmer/4000 Å break. The break is also a powerful diagnostic in stellar population studies (e.g. Hamilton 1985; Balogh et al. 1999; Kauffmann et al. 2003a).

For galaxies beyond $z \sim 1.5$ the break shifts into the NIR, where the combination of high sky background and strong atmospheric absorption bands complicates continuum studies of galaxies. Recently new NIR spectrographs on 8-10 meter class telescopes have improved our access to the NIR regime significantly. This is demonstrated by the first possible detections of rest-frame optical breaks by van Dokkum et al. (2004) and Simpson et al. (2004) with KECK/NIRSPEC and SUBARU/CISCO respectively. Furthermore, the large instantaneous wavelength coverage offered by GNIRS on Gemini-South (see e.g. van Dokkum et al. 2005) allows, for the first time, systematic continuum studies of galaxies at $z > 2$.

In this paper we present and study the rest-frame optical continua of three DRGs, of which only one had a spectroscopic redshift prior to the observations. The data are presented in §2. In §3 we fit the spectra with evolutionary synthesis models and compare the spectra with the broadband SEDs. In §4 we use spectral diagnostics to obtain stellar population properties. We present a direct comparison with other high-redshift and low-redshift galaxies in §5. We end with a summary and conclusions in §6. Throughout the paper we assume a ΛCDM cosmology with $\Omega_{\mathrm{m}} = 0.3$, $\Omega_{\Lambda} = 0.7$, and $H_0 = 70$ km s^{-1} Mpc^{-1}. All broadband magnitudes are given in the Vega-based photometric system.

2. DATA

2.1. *Target selection and photometry*

The three studied galaxies lie in the field of MS1054-03, the CDF-South and the extended HDF-South respectively. All fields have deep NIR imaging and accurate photometry in several optical-to-NIR bands. The MS1054-03 field is observed as part of the "ultra-deep" Faint InfraRed Extragalactic Survey (FIRES) and the photometry is described by Förster Schreiber et al. (2006). The Great Observatories Origins Deep Survey (GOODS; Giavalisco et al. 2004) provides deep data of the CDF-South. The optical-to-NIR photometry that we used as part of this work will be described by Wuyts et al. (2006, in prep.). The photometry of the extended HDF-South is part of the new MUlti-wavelength Survey by Yale-Chile (MUSYC; Gawiser et al. 2005, Quadri et al. in prep).

The three galaxies are chosen on the basis of their K magnitude, red $J_s - K_s$ color ($J_s - K_s > 2.3$; Franx et al. 2003), and redshift between 2.1 and 2.7. To avoid a bias towards galaxies with strong UV emission, we did not require that a previously measured spectroscopic redshift was available, and two out of three galaxies presented in this paper were selected on basis of their photometric redshift. MS1054-1319 was the only galaxy which had a spectroscopic redshift ($z = 2.423$) prior to these NIR observations, derived from both the Lyα and Hα emission lines (van Dokkum et al. 2003, 2004). The NIR spectrum of CDFS-695 studied in this paper has already been presented by van Dokkum et al. (2005), who give an emission line redshift of 2.225.

Where possible the broadband fluxes were corrected for emission line fluxes. The observed infrared photometry for CDFS-695 is adjusted using the line measurements presented by van Dokkum et al. (2005). The emission line corrections are crucial to interpret the broadband photometry for this galaxy, as they account for 0.05, 0.17 and 0.25 mag of the total J, H and K broadband magnitudes respectively. Hence, after corrections CDFS-695 does not satisfy the $J_s - K_s > 2.3$ criterion. For this galaxy we have no observed optical spectrum. Fortunately, CDFS-695 is also part of the *K20 survey*, and from the spectrum presented by Daddi et al. (2004a) we conclude that the emission lines barely contribute to the observed optical broadband fluxes. Thus, no corrections are made to the broadband observed optical magnitudes of CDFS-695, but the photometric errors are increased by 0.05 mag. For MS1054-1319 the emission line correction were derived by van Dokkum et al. (2004), who find contributions of 0.1, 0.02, 0.03, 0.04 mag to the broadband fluxes of B, J, H and K respectively, and an increase of the photometric error of V and I by 0.05 mag. For HDFS-5710, no emission lines are detected in the NIR spectrum and therefore no correction is applied.

2.2. *Observations*

Table 1 summarizes the observations. Two out of three galaxies presented in this paper were observed with GNIRS on Gemini-South in September 2004: CDFS-695 and HDFS-5710 (program GS-2004B-Q-38). We used GNIRS in cross-dispersed mode, in combination with the short wavelength camera with the 32 l/mm grating (R=1000) and the $0\farcs675$ by $6\farcs2$ slit. In this configuration we obtained a wavelength coverage of 1.0 – 2.4 μm, divided over 6 orders. Conditions on September 2 and 3, during which we observed CDFS-695, were relatively good with a seeing of $0\farcs7$ in K and mostly clear sky. HDFS-5710 was observed on September 6 through intermittent clouds, and the seeing varied from $0\farcs7$ – $1\farcs3$.

We observed the galaxies following an ABA′B′ on-source dither pattern. In this way we can use the av-

TABLE 1
OBSERVATIONS

id	K_s	V	$J_s - K_s$	Instrument	date	$\lambda_{\rm range}$	Exp(min)	$R_{\rm spec}$	Seeing($''$)
MS1054-1319	19.01	24.21	2.58	KECK/NIRSPEC	2003/01/22	2.05-2.47	90	1600	0.″9
						1.28-1.56	60	1600	0.″9
					2004/02/11	1.23-1.55	105	1600	0.″8
						1.50-1.74	60	1600	0.″8
				VLT/ISAAC	2004/04/25	1.82-2.50	81	600	0.″7
						2.14-2.26	165	3900	0.″7
CDFS-695	19.12	23.71	2.33	GEMINI-S/GNIRS	2004/09/02-03	1.0-2.4	92	1000	0.″7
HDFS-5710	19.31	25.53	2.47	GEMINI-S/GNIRS	2004/09/06	1.0-2.4	210	1000	1.″0

erage of the previous and successive exposures as the sky frame. The offset between A and A′ ensures that different parts of the detector are used for sky subtraction. To optimize the signal-to-noise ratio (S/N) of the extracted one-dimensional (1D) spectrum, the shift between A and A′ should be larger than the area over which the spectrum is extracted. Compared to the standard ABBA pattern, this method decreases the noise by about 13 % in the sky-subtracted frames.

We complemented the GNIRS spectra with the spectrum of MS1054-1319 obtained with NIRSPEC on Keck (McLean et al. 1998). We observed MS1054-1319 during two runs using the N4 filter and medium dispersion mode (1.23-1.55 μm, R=1600), which is especially useful to target the region around the optical break for $z \sim 2.5$ galaxies. The first run in January 2003 was characterized by cloudy weather and a typical seeing of 0.″9 in K (van Dokkum et al. 2004). The conditions during the second run in February 2004 were somewhat better with a seeing of 0.″8. To extend the wavelength coverage for this galaxy, we complement the N4 coverage by H and K band spectra obtained with NIRSPEC on KECK and ISAAC on the VLT. For details on these observations see Table 1. The NIRSPEC and ISAAC spectra were taken at three dither positions (ABC), as the slit length of both instruments is longer than for GNIRS. Similar to the ABA′B′ pattern we can use the average of the previous and following exposures as sky frame.

All targets were acquired by blind offsets from nearby stars. With NIRSPEC the alignment was checked and corrected if needed before every individual 900 s exposure. Furthermore, at each dither position a separate spectrum was taken of the offset star to determine the expected position of the object spectrum on the detector. As GNIRS and ISAAC have better pointing stability there was no need for re-acquisition after each individual exposure, and acquisition checks were performed approximately every hour. The total exposure times of all objects and modes are listed in Table 1.

After each observing sequence, we observed an AV0 star near the target. These spectra are used in the reduction to correct for detector response and atmospheric absorption.

We note that other targets were also observed during these runs. However, the galaxies discussed here are the only ones for which we specifically attempted to measure the continuum rather than just emission lines.

2.3. *Reduction of GNIRS spectra*

The reduction of the NIRSPEC spectra of MS1054-1319 is described by van Dokkum et al. (2004). The ISAAC spectra of MS1054-1319 were reduced in a similar way as the NIRSPEC spectra. For the GNIRS data reduction of CDFS-695 and HDFS-5710 we developed a suite of custom scripts to perform the following steps. We started the reduction by removing a bias pattern. The pattern repeats itself every 8 columns, differently in each quadrant. It was modeled by fitting a constant along the vertical direction in regions where no spectrum is present, and removed over the whole detector. We also corrected for persistence from the acquisition image on the detector.

Cosmic rays were removed as follows. First, we removed the sky from the science frames by subtracting the average of the previous and next exposure. For additional sky-subtraction we have to straighten the orders, which follow curved paths on the detector. We determined the position of the object spectrum in each row of each order by tracing the spectrum of a bright star. Next, we straightened the orders by integer pixel shifts (to retain the cosmic ray shapes), using the expected object positions. Because of the small slit length, there is not enough 'empty' sky left to remove the remaining sky by fitting lines along the spatial direction. However, the negative object spectrum should cancel its positive counterpart, and any residual sky was removed by requiring that the biweight mean (Beers, Flynn, & Gebhardt 1990) along the spatial direction is zero at every wavelength. Next, we run L.A.Cosmic (van Dokkum 2001) on the sky-free frames to identify the cosmic rays. The resulting cosmic ray masks were convolved by a boxcar to exclude neighboring pixels. The masks of the different orders were transformed back to the original shape of the spectrum without interpolation and combined to one cosmic ray mask for each individual exposure. Throughout the following description, the cosmic ray mask will be transformed in the same way as the science frames.

We continued with the original raw frames and performed the same steps as described above to remove the sky, only this time we allowed interpolation when straightening the orders. For each exposure and each order, a 1D noise frame was made from the subtracted sky. This noise frame was used to identify dead and hot pixels, which were added to the mask.

Next, the orders of each frame were wavelength calibrated using arc lamp frames. The calibrations were checked and if necessary corrected using skylines. Corrections for the instrumental response function and at-

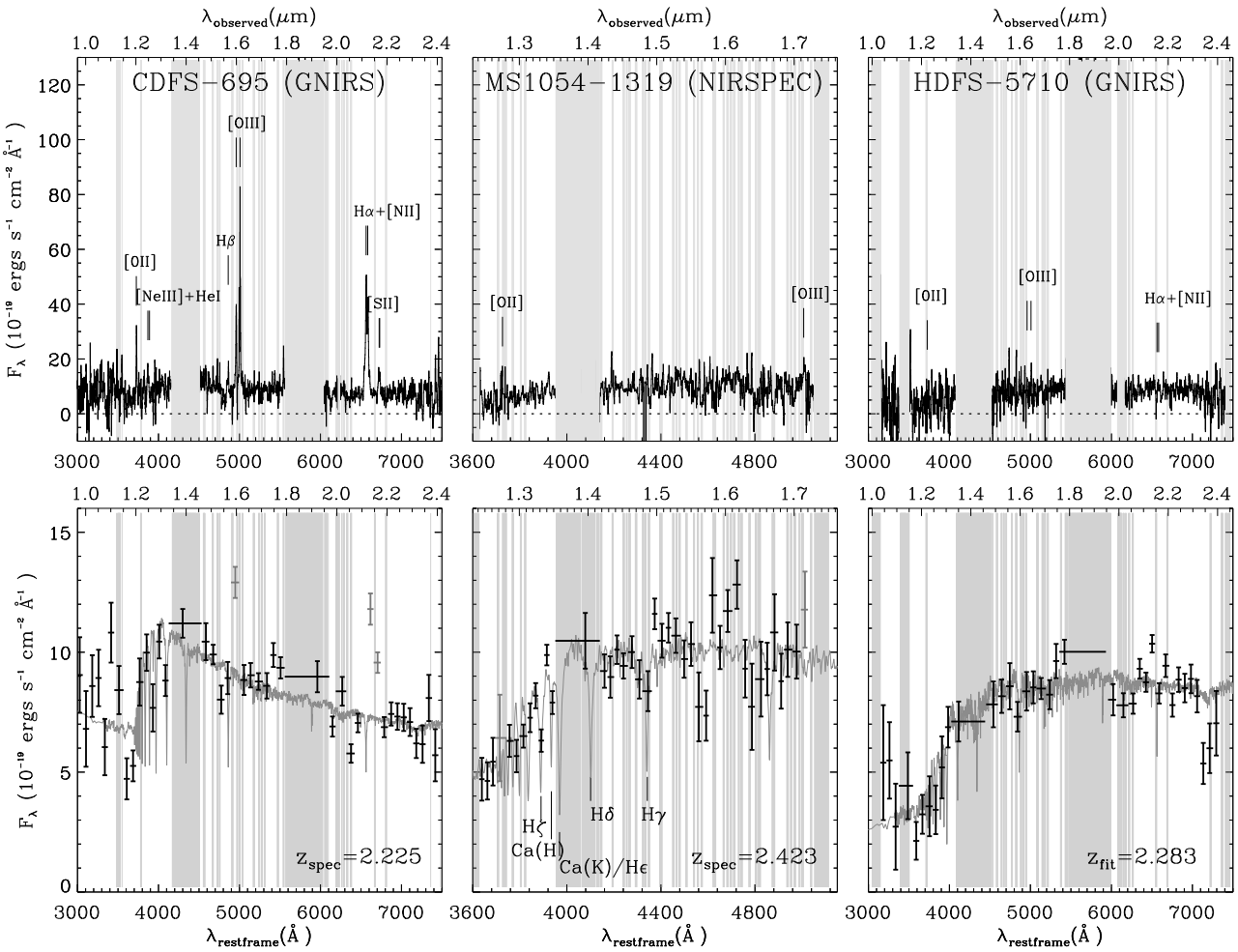

FIG. 1.— Extracted one-dimensional spectra (*upper panels*) and their binned version (*lower panels*) for CDFS-695 (*left*), MS1054-1319 (*middle*) and HDFS-5710 (*right*). The presented original 1D spectra (upper panels) are smoothed by a boxcar of 25 Å and 13 Å (observed frame) for GNIRS and NIRSPEC spectra respectively. Bad atmospheric regions or wavelengths that are heavily contaminated by skylines are indicated in *light grey*. Bins that include emission line fluxes are plotted in *grey* as well. The best fit template spectra (*dark grey*) are overplotted (see Table 2). For each galaxy a break is detected between 3650 and 4000 Å.

mospheric absorption were applied by dividing by the response spectrum. This spectrum was created from the observed spectrum of an AV0 star, which was divided by the spectrum of Vega. Residuals from Balmer absorption features in the spectrum of the AV0 star were removed by interpolation. The spectrum of the AV0 star was reduced in the same way as the science frames.

The different exposures were combined for each order, excluding cosmic rays and outliers as identified in the masks. Finally the orders were combined, properly weighting overlapping regions using the response function. In the entire procedure pixels were interpolated only once, to minimize smoothing and noise correlations in the final frames.

2.4. *Extraction of 1 dimensional spectra*

For all three galaxies the 1D spectrum was extracted by summing all lines (along the wavelength direction) with a mean flux $> 0.25 \times$ the flux in the central row, using optimal weighting. In addition, a 'low-resolution' (binned) spectrum was extracted as follows. The pixels were sampled along the wavelength direction in each line of the two-dimensional (2D) spectrum using the biweight estimator. Thus we created a binned spectrum for each line of the 2D spectrum. Hereafter the lines with a mean flux $> 0.25 \times$ the flux in the central line were added corresponding to their weighting factors. This procedure gives a higher S/N in the final low resolution spectrum than binning the original extracted 1D spectrum.

Regions with low or variable atmospheric transmission or with strong sky line emission were excluded. For CDFS-695 and HDFS-5710 observed with GNIRS, we defined these regions as those with less than 5% of the maximum transmission and with sky line intensities of 30% or more of the strongest line. For MS1054-1319 observed with NIRSPEC and ISAAC, these criteria were <30% and >25%, respectively. For MS1054-1319 the spectra were sampled in 30 pixel bins (∼80 Å), and the other two galaxies were sampled in bins of 50 pixels (∼250 Å). Rather than to vary the number of pixels that contribute to each wavelength bin (i.e. excluding bad wavelength regions), the width was adjusted such that each bin contains 30 or 50 'good' pixels.

For MS1054-1319 we combined the NIRSPEC and ISAAC spectra of different but overlapping wavelength coverages. Adding 2D spectra would have decreased the S/N as there is a difference in seeing and sampling of instruments. Instead we combined the different spectra in the following way. First, we extracted a low resolution spectrum for each individual 2D spectrum, by using the same bins and a common mask for excluding regions of poor atmospheric transmission or with strong sky lines. These spectra were scaled by minimizing χ^2 in the overlapping regions and thereafter combined. These scaling factors were used to combine the 'high resolution' 1D spectra as well. Spectra of different wavelength coverages without overlapping regions were scaled using the total broadband H and K magnitudes. To scale the spectra, we modeled the continuum by fitting a straight line to the low resolution spectrum, excluding bins that may contain emission lines. The modeled continuum was converted to F_ν and thereafter convolved with the appropriate filter-curve and normalized using the emission line corrected total fluxes. The GNIRS spectra of HDFS-5710 and CDFS-695 were scaled in the same way, but as the wavelength coverage is not divided over different bands, we used an error-weighted average scale factor obtained from the broadband H and K magnitudes to tie the spectrum to the broad band photometry. In this procedure, we did not use the broadband J magnitude because the Balmer/4000 Å break complicates the modeling of the continuum in this band.

The 1D original and low resolution spectra are presented in Fig. 1. For MS1054-1319 we only show the area around the break observed with NIRSPEC, which has continuous coverage. For each galaxy an optical break is detected. This is no coincidence, as the selection criterion of $J_s - K_s > 2.3$ was introduced to identify galaxies with prominent 4000 Å and/or Balmer breaks. There are even indications that some individual absorption features are detected for MS1054-1319 (Hζ and Ca(H)) and CDFS-695 (Ca and Hδ). The sensitivity of the spectra of CDFS-695 and HDFS-5710, observed with GNIRS, decreases in the blue, which is reflected in the error bars in Fig. 1. The outliers bluewards of the break in CDFS-695 are caused by residual bias patterns which cannot be properly removed.

In the spectrum of CDFS-695, we clearly detect several emission lines that are labeled in Fig. 1. The analysis of these emission lines is presented by van Dokkum et al. (2005). For MS1054-1319 we observe two possible emission lines ([O II] at 3727 Å and [O III] at 5007 Å) in the combined $N4$ and H band spectra. This galaxy also has detected Hα and [N II] emission in its K-band spectrum (van Dokkum et al. 2004). Strikingly, for HDFS-5710 no emission lines were detected at all. Note that the galaxy without emission line detections appears to have the strongest break (HDFS-5710), and that the galaxy with the strongest lines (CDFS-695) has the weakest break. In § 4.2 we will investigate this relation between the break strength and emission lines in more detail.

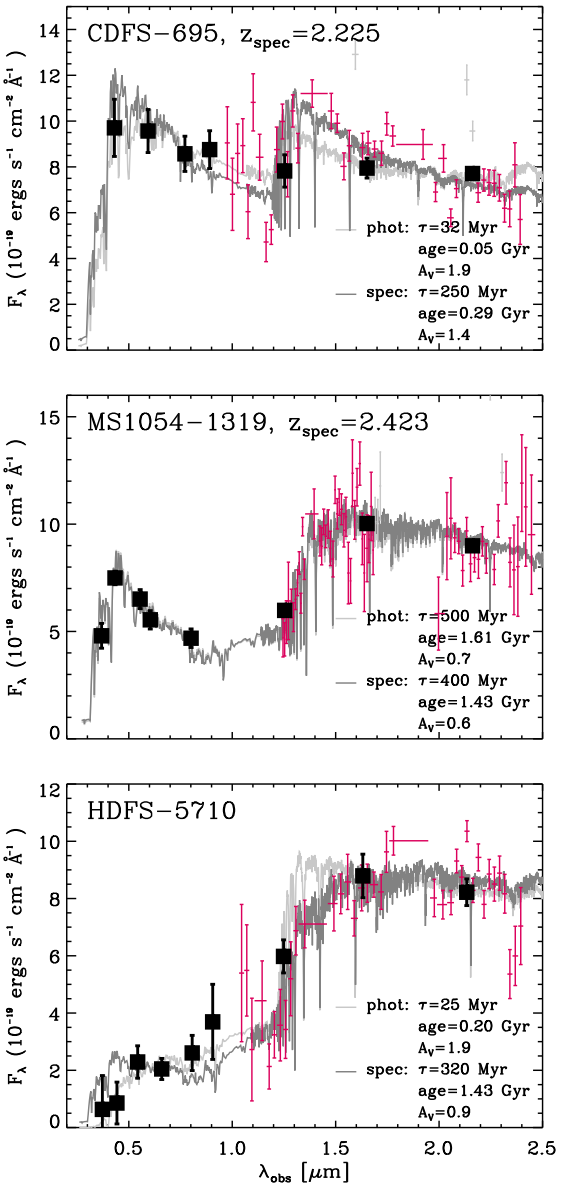

FIG. 2.— Broadband photometry together with the observed and modeled spectra for CDFS-695 (*upper panel; B, V, I, z, J, H, & K*), MS1054-1319 (*middle panel; U, B, V, R, I, J, H, & K*), and HDFS-5710 (*lower panel; U, B, V, R, I, z, J, H, & K*). The error bars represent the 1σ uncertainties of the flux measurements. The bins that are contaminated by emission line fluxes, and thus not included during fitting are plotted in grey. The best fits to just the photometry (*light grey*) and to the spectra in combination with the rest-frame UV bands (*dark grey*) are overplotted. For MS1054-1319 and CDFS-695 the redshift was fixed to the emission line redshift during the fitting procedure, while for HDFS-5710 z was a free parameter. The τ, A_v, and *age* (see §3.1) of the best fit are listed in the panels.

3. SPECTRAL MODELING

Modeling the broadband photometry is a popular method to study the properties of high-redshift galaxies (e.g. Sawicki & Yee 1998; Papovich et al. 2001; Shapley et al. 2001; Förster Schreiber et al. 2004). Unfortunately, the modeling results suffer from degeneracies between age, dust and the star formation timescale. In this section we investigate the additional constraints provided by the rest-frame optical spectra.

3.1. *Fitting procedure and results*

We used synthetic spectra by Bruzual & Charlot (2003) to model our data. We selected a stellar population with a Salpeter (1955) initial mass function (IMF)

TABLE 2
Modeling Results

id	τ Gyr	age Gyr	A_V mag	z^a	$\chi^2_{\rm min}$ [b]	$\chi^2_{1\sigma}$	$\chi^2_{2\sigma}$	N[c]	$M_\star$ 10^{11} $M_\odot$	SFR $M_\odot yr^{-1}$	SFR/$M_\star$ 10^{-11} yr^{-1}
CDFS-695											
phot	$0.03^{+9.97}_{-0.02}$	$0.05^{+0.15}_{-0.00}$	$1.9^{+0.2}_{-0.4}$	-	0.77	1.46	3.46	3	$0.8^{+0.3}_{-0.1}$	722^{+874}_{-662}	932^{+1276}_{-854}
spec	$0.25^{+9.75}_{-0.22}$	$0.29^{+0.28}_{-0.18}$	$1.4^{+0.1}_{-0.2}$	-	2.78	2.85	2.95	39	$1.3^{+0.3}_{-0.3}$	284^{+100}_{-206}	226^{+85}_{-143}
MS1054-1319											
phot	$0.50^{+0.50}_{-0.18}$	$1.61^{+0.79}_{-0.47}$	$0.7^{+0.2}_{-0.1}$	-	1.28	2.10	3.20	4	$4.2^{+1.8}_{-1.3}$	47^{+34}_{-11}	11^{+6}_{-1}
spec	$0.40^{+0.10}_{-0.08}$	$1.28^{+0.16}_{-0.14}$	$0.7^{+0.2}_{-0.1}$	-	1.59	1.67	1.73	61	$3.5^{+0.6}_{-0.4}$	48^{+25}_{-12}	14^{+6}_{-2}
HDFS-5710											
phot	$0.03^{+9.98}_{-0.01}$	$0.20^{+2.80}_{-0.15}$	$1.9^{+1.1}_{-1.9}$	$2.28^{+0.15}_{-1.30}$	0.52	1.90	2.83	4	$3.2^{+2.1}_{-3.0}$	4^{+1417}_{-4}	1^{+546}_{-1}
spec	$0.32^{+0.18}_{-0.16}$	$1.43^{+1.32}_{-0.93}$	$0.9^{+1.1}_{-0.6}$	$2.283^{+0.028}_{-0.020}$	2.21	2.37	2.57	38	$4.0^{+1.7}_{-0.8}$	19^{+165}_{-15}	4^{+33}_{-3}

[a]The redshifts of CDFS-695 and MS1054-1319 are fixed to $z_{H\alpha}$=2.225 and $z_{H\alpha}$=2.423 respectively.
[b]χ^2 is given per degree of freedom. The 1σ and 2σ values correspond to the 68% and 95% confidence levels, derived from the Monte Carlo simulations described in §3.1
[c]Number of degrees of freedom

between 0.1-100 $M_\odot$, a solar metallicity, and based on the Padova 1994 evolutionary tracks. We adopted the reddening law of Calzetti et al. (2000) and corrected for intergalactic attenuation by the Lyα forest using the prescriptions of Madau et al. (1996). For a discussion about the choice of the model parameters and the effects of their variations, see Förster Schreiber et al. (2004).

The star formation history is parametrized by an exponentially declining function with characteristic time scale τ. Synthetic spectra were constructed for a grid of 31 different τ's between 10 Myr and 10 Gyr, 24 different ages between 10 Myr and 3 Gyr (and always restricted to be less than the age of the universe at a given redshift), redshifts in steps of $\Delta z = 0.001$, and 31 extinction values (A_V) between 0 and 3 mag. For MS1054-1319 and CDFS-695, the redshift was fixed to the emission line redshift.

The templates were sampled in the same bins as the observed spectra, thus wavelength regions with bad atmospheric transmission and strong skylines in the observed spectra were excluded in the synthetic spectra as well. Additionally, bins that were contaminated by emission line fluxes ([OIII], Hα, [NII] and [SII]) were excluded during fitting, as the models do not include emission by the ionized interstellar medium. To extend our wavelength coverage to the rest-frame UV, we complemented the observed spectra with the optical photometry. The broadband fluxes of the synthetic spectra were derived by integrating the flux accounting for the filter curves. The minimum error in the broadband fluxes was set to 0.05 mag to account for absolute calibration uncertainties.

The spectra in combination with the rest-frame UV photometry were fitted by using least-square minimization (χ^2). We performed 200 Monte Carlo simulations to calibrate the confidence levels. For these simulations we varied the fluxes randomly within the errors, assuming a Gaussian distribution, and followed the same procedure as applied to the original data. The 1σ and 2σ confidence levels are derived from the χ^2 values of the original fit which enclose the best 68% and 95% of the simulations (see Papovich et al. 2001). These χ^2 values per degree of freedom are listed in Table 2.

The best spectral fits are shown in Fig. 2. The τ, age, A_V, redshift, stellar mass, star formation rate (SFR) and χ^2 corresponding to these fits are listed in Table 2. All allowed combinations of z, τ, A_V and *age* are presented as 1σ and 2σ confidence levels (color contours) in Fig. 3.

3.2. *Continuum redshifts*

To test the accuracy of the redshift obtained by spectral fitting, both CDFS-695 and MS1054-1319 were refit with z as a free parameter. The spectra of these galaxies give remarkably good solutions for z. This is illustrated in Fig. 4. For MS1054-1319, which has an Hα and Lyα redshift of 2.423 and 2.424 respectively (van Dokkum et al. 2003, 2004), we find $z_{\rm fit} = 2.423^{+0.002}_{-0.003}$. For CDFS-695 which has an Hα and Lyα redshift of 2.225 and 2.223 (van Dokkum et al. 2005; Daddi et al. 2004a), we find $z_{\rm fit} = 2.21^{+0.11}_{-0.03}$. This galaxy has a secondary solution for redshift ($z \sim 2.32$) that is probably caused by mis-identification of the absorption features in this spectrum.

The uncertainty on the derived value for the redshift is decreased significantly compared to only using the broadband fluxes. The green lines and shaded areas in Fig. 4 indicate the 1σ redshift range allowed by the photometry, using Bruzual & Charlot (2003) models (see confidence levels in Fig. 3). The purple lines and surrounding shaded areas are obtained by fitting linear combinations of theoretical and empirical templates to the broadband photometry, following the method described by Rudnick et al. (2001, 2003). The uncertainty on the redshifts are decreased by a factor of 6-50 when including the spectrum.

For HDFS-5710 which is the only galaxy without an emission line redshift, spectral modeling yields $z_{\rm fit} = 2.283^{+0.028}_{-0.020}$ (see Fig. 4). This result illustrates the potential of NIR spectroscopy to measure redshifts of $z > 2$

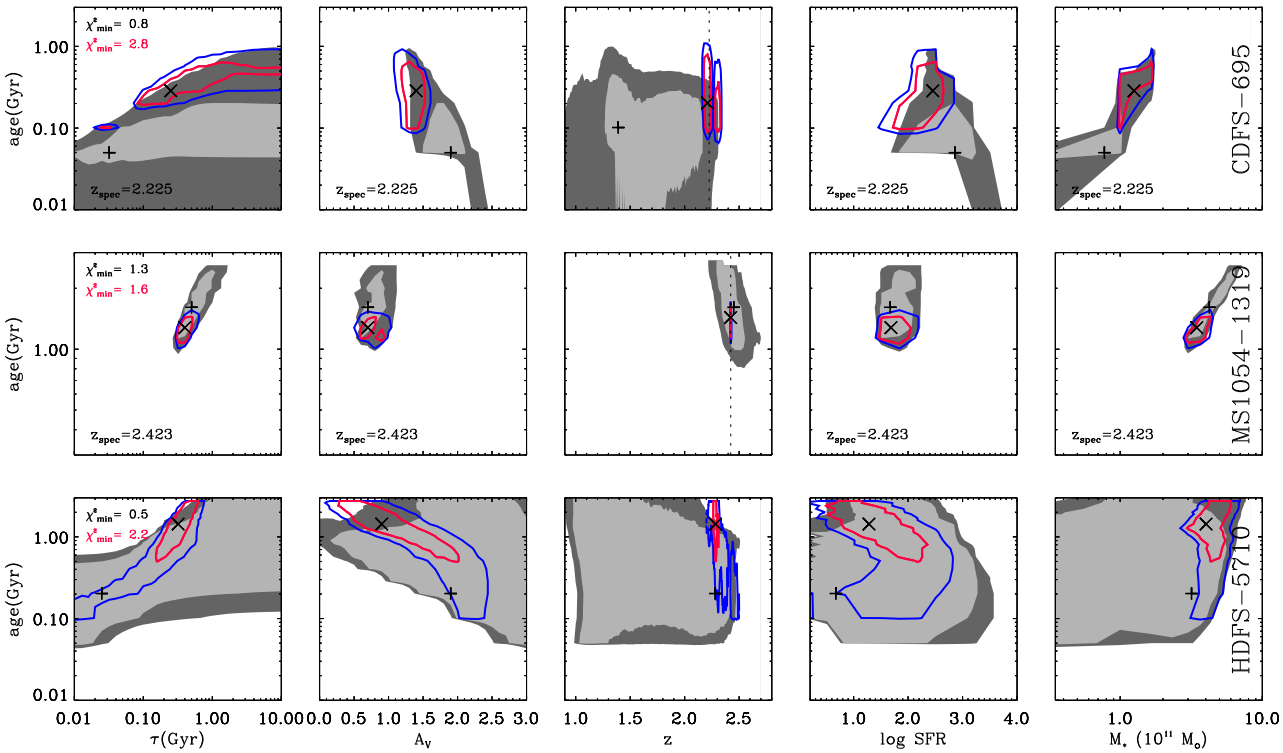

FIG. 3.— Comparison of modeling results between the spectrum plus rest-frame UV broadband fluxes and the broadband SED for CDFS-695 (*upper panels*), MS1054-1319 (*middle panels*) and HDFS-5710 (*lower panels*). The best-fit solutions and their 1σ and 2σ confidence levels are presented by the crosses and color contours for the spectrum together with the optical photometry, and pluses and filled greyscale contours for solely the optical-to-NIR photometry. For MS1054-1319 and CDFS-695, the redshift was fixed to $z_{\rm H\alpha}$ to derive τ, *age*, A_V, SFR and stellar mass. The dotted lines in the age versus z plots indicate the emission line redshifts. For HDFS-5710 the redshift was a free parameter when deriving all properties. The χ^2 value of the best fit solution is given in the left panels, in red for the spectral fit and in black for the photometry fit. This figure shows that the spectrum improves the constraints on all properties substantially. In addition, the modeled redshifts for CDFS-695 and MS1054-1319 are remarkably accurate.

galaxies that are faint in the rest-frame UV and have no detectable emission lines.

3.3. *Comparison to broadband SEDs*

To investigate if the spectra confirm and improve the constraints on the stellar populations properties, we re-fitted the photometry of the three galaxies, ignoring the spectral information. The comparison between the allowed solutions for the input parameters z, τ, age and A_V, and the output parameters stellar mass and SFR for the spectra and broadband SED is presented in Fig. 3. The corresponding values are listed in Table 2. The best-fit templates to the spectra and photometry, and the best fits to the photometry alone are shown in Fig. 2.

Fig. 3 shows that the spectra greatly improve the constraints on the modeled properties, for all three galaxies. Most of the 1σ solutions to the spectra fall within the 2σ confidence levels of the photometry. However, most of the 1σ confidence regions of the photometric fits are, within 2σ, not allowed by the spectral fits. For example, while the photometry of CDFS-695 still allows a wide range in dust content and age, the solutions dustier than 1.6 mag and younger than 0.1 Gyr are ruled out by the spectrum. Even MS1054-1319, for which the properties are already well-constrained by the photometry, the spectrum decreases the 1σ confidence interval of age and τ by a factor 7-8. And finally, for HDFS-5710 the largest gain is achieved by the better constrained redshift. Also, solutions with τ longer than 700 Myr are ruled out by the spectrum.

The normalized χ^2 values per degree of freedom for the fits to the broadband photometry are lower than those for the fits including the NIR spectroscopy. However, the difference between the χ^2 of the best fit and the 1σ and 2σ confidence intervals are smaller for fits including the NIR spectra (see Table 3), which result in the tighter constraints. One possible cause for the difference in minimal χ^2 of the best photometric and spectral fits is that χ^2 statistics are very sensitive to the data uncertainties. The photometric errors may be overestimated or the spectral errors may be underestimated. Another cause could be template mismatch, which can become more problematic with more detailed spectroscopic information.

To test the robustness of our results we repeated the fitting procedure for MS1054-1319, artificially decreasing the errors on the photometry by a factor of 2 and increasing the errors on the spectra by a factor of 2. The allowed ranges for A_V, age and τ are slightly increased and reduced for the spectra and photometry respectively, but even in this extreme case inclusion of the spectra still improves the constraints on the stellar populations.

3.4. *Discussion of modeling results*

Our fitting results show that including the NIR spectra when fitting the broadband fluxes sets tighter constraints

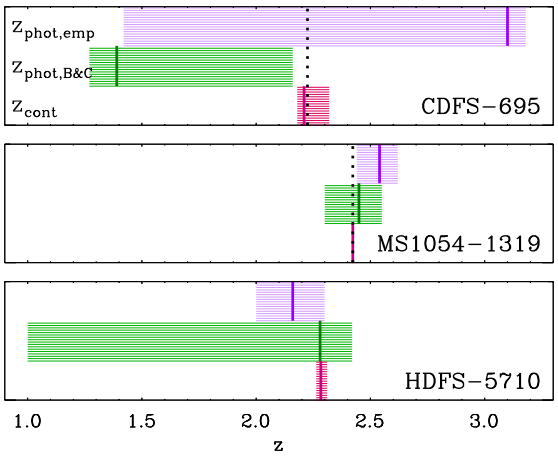

FIG. 4.— Comparison between continuum redshift, broadband photometric redshift and the emission line redshift. The best-fit redshift and its 1σ confidence interval to the NIR continuum together with the optical photometry is indicated by the red line and surrounding shaded area respectively. The green thick line and the surrounding shaded area present the best-fit redshift and its allowed 1σ range when fitting the optical-to-NIR broadband photometry by Bruzual & Charlot (2003) models. The best-fit redshift and its 1σ uncertainty obtained when fitting the photometry by linear combinations of empirical and theoretical galaxy templates (Rudnick et al. 2001, 2003) is shown by the purple thick lines and shaded areas. The emission line redshift, if present, is indicated by the black dotted line. This diagram illustrates that the continuum shape is powerful in obtaining accurate and well-constrained redshifts.

on stellar population properties and reduces degeneracies between age, extinction and the SFH. This is mainly due to the measurement of the shape and strength of the optical break. We conclude that the spectral shape in combination with the photometry is more powerful than the broadband photometry alone in tracing the properties of stellar populations in high redshift galaxies.

The DRGs studied here span a wide range in their derived properties, consistent with results of larger samples based on modeling of their broadband SEDs (e.g. Förster Schreiber et al. 2004; Labbé et al. 2005). Their SFH, reddening and age are quite different, ranging from CDFS-695 which is about 0.2 Gyr old and is forming a few hundred solar masses a year, to HDFS-5710 and MS1054-1319 which are both best fitted by a stellar population of 1.4 Gyr old and are forming a few tens of solar masses a year.

Labbé et al. (2005) divided their DRG sample into dusty starburst and "red and dead" galaxies based on the observed NIR and IR colors ($I-K$ and $K-4.5\mu$). To compare the DRGs presented in this work with those of Labbé et al. (2005), we measured the same colors by extrapolating the best spectral fit to the rest-frame NIR. All three galaxies fall in the dusty star-forming part of the plot, although their locations move closer towards the "red and dead" part, when going from CDFS-695 to MS1054-1319 to HDFS-5710.

4. SPECTRAL DIAGNOSTICS

In the previous section we studied the spectra by comparing them to models. The break appeared to be the driving feature behind the improved modeling constraints. In this section, we take a different approach by measuring the break directly, and use this feature in combination with Hα to constrain the star formation histories of the galaxies.

4.1. *Break indices*

The Balmer and 4000 Å break are often treated as one feature, owing to their similar locations and the fact that they partially overlap. However, the breaks originate from different physical processes, and behave differently as populations age. Both breaks are due to absorption in the atmosphere of stars. The 4000 Å break arises because of an accumulation of absorption lines of mainly ionized metals. As the opacity increases with decreasing stellar temperature, the 4000 Å break gets larger with older ages, and is largest for old and metal-rich stellar populations. The metallicity is of minor influence for ages less than 1 Gyr (Bruzual & Charlot 2003). There are several definitions introduced to quantify the strength of the 4000 Å break. Bruzual (1983) proposed $D(4000)$, which measures the ratio of the average flux density F_ν in the bands 4050-4250 Å and 3750-3950 Å around the break. Because of the broad regions, this index is fairly sensitive to reddening by dust. To reduce this effect, Balogh et al. (1999) defined a new index $D_n(4000)$, based on smaller continuum regions (3850-3950 Å, 4000-4100 Å).

The Balmer break at 3646 Å marks the termination of the Hydrogen Balmer series, and is strongest in A-type stars. Therefore the break strength does not monotonically increase with age but reaches a maximum in stellar populations of intermediate ages (0.3-1 Gyr). The strength of the Balmer sequence can be best measured from the individual Balmer lines, such as Hδ. However, as our spectra do not allow the measurement of this feature, we use the strength of the Balmer break (D_B), which we define as the ratio of the average flux density F_ν in the bands 3500-3650 Å and 3800-3950 Å around the break. The large regions are not optimal, but are a trade-off between dust-dependence and having sufficient S/N using the spectra of high redshift galaxies. This index is also partially influenced by the 4000 Å break. Nevertheless, the age-dependence of D_B is very similar to that of Hδ.

We determined $D_n(4000)$ and D_B for the three DRGs. The average flux in the regions around the breaks is measured in the same way as we extracted the binned spectra. For MS1054-1319 it was impossible to measure the flux redwards of the 4000 Å break, as the defined region is entirely covered by an atmospheric band. Therefore we measured $D(4000)$ and used the Bruzual & Charlot (2003) models to derive $D_n(4000)$ for this galaxy. When converting the indices we allowed an A_V between 0 and 3 and all three star formation histories to determine the uncertainty. We note that this only slightly increases the uncertainty as for the measured break strength of MS1054-1319 the correlation between $D(4000)$ and $D_n(4000)$ is not very dependent on dust or the star formation history.

The break measurements are listed in Table 3 and shown in Fig. 5. The behavior of the Balmer and 4000 Å break with age for $\tau_{10\mathrm{Myr}}$, $\tau_{320\,\mathrm{Myr}}$ and $\tau_{10\mathrm{Gyr}}$ (which is comparable to constant star formation for galaxies at $z>2$) models are overplotted for the first 3 Gyr. This

TABLE 3
Spectral features

id	$W_{H\alpha}$(Å)[a]	$D_n(4000)$	D_B
CDFS-695	99±10[b]	$1.17^{+0.14}_{-0.09}$	$1.84^{+0.24}_{-0.15}$
MS1054-1319	19±4[c]	$1.28^{+0.16}_{-0.04}$	$1.69^{+0.24}_{-0.20}$
HDFS-5710	< 10	$1.38^{+0.47}_{-0.33}$	$2.40^{+0.67}_{-0.43}$

[a]Uncorrected for Balmer absorption
[b]van Dokkum et al. (2005)
[c]van Dokkum et al. (2004)

figure is useful for discriminating between different star formation histories, as it provides a clear illustration that (near-)constant star formation models are not able to produce a large break within 3 Gyr. However, if a galaxy is extremely dusty, reddening can mimic a very large break. All three galaxies fall on the model curves. For MS1054-1319 the break implies an age of about 1 Gyr. The break of CDFS-695 reveals a younger stellar population. The large Balmer break for HDFS-5710 suggests that this galaxy is in a post-starburst phase. Unfortunately the errors are too high to draw firm conclusions from these diagnostics.

4.2. *Comparison to Hα equivalent width*

In addition to the break, the equivalent width of Hα ($W_{H\alpha}$) can help discriminate between dusty starbursts and evolved stellar populations. As $W_{H\alpha}$ is sensitive to the ratio of the current and past star formation it is an independent measure of the star formation history and the age of a stellar population.

The $W_{H\alpha}$ of MS1054-1319 and CDFS-695 were measured by van Dokkum et al. (2004, 2005). For HDFS-5710, no Hα emission line is detected, and thus we give an 3σ upper limit for $W_{H\alpha}$ using the redshift derived in Sect. 3, and assuming a FWHM of 500 km/s. To check for a possible Hα detection within the 2σ allowed redshift range, we measured the S/N of a possible line for redshifts between 2.2 and 2.5 (in steps of 0.001). For none of these redshifts do we find a detection exceeding the limits derived for the best fitting redshift. The values of $W_{H\alpha}$ for all galaxies are listed in Table 3.

In Fig. 6a we plot $W_{H\alpha}$ as a function of $D_n(4000)$ for the galaxies and different models ($\tau_{50\mathrm{Myr}}$, $\tau_{320\,\mathrm{Myr}}$ and $\tau_{10\mathrm{Gyr}}$). The plotted $W_{H\alpha}$ are corrected for a Balmer absorption with an equivalent width of 4 ± 1Å, which is typical for stellar populations with ages of 0.5-2.0 Gyr (Förster Schreiber et al. 2004). The model tracks are derived from the Kennicutt (1998) law, which relates the luminosity of Hα to the SFR, in combination with the Bruzual & Charlot (2003) models. These tracks illustrate that neither a large break nor a low $W_{H\alpha}$ can be produced for $\tau_{10\mathrm{gyr}}$ or CSF models within 3 Gyr.

Fig. 6a illustrates that the three galaxies are at different stages in their stellar evolution. The undetected Hα of HDFS-5710 is consistent with the large break, as both imply an evolved stellar population. Furthermore we note that the SFR from the continuum fits (see §3.1) of 19 $M_\odot$/yr is in agreement with the SFR upper limit

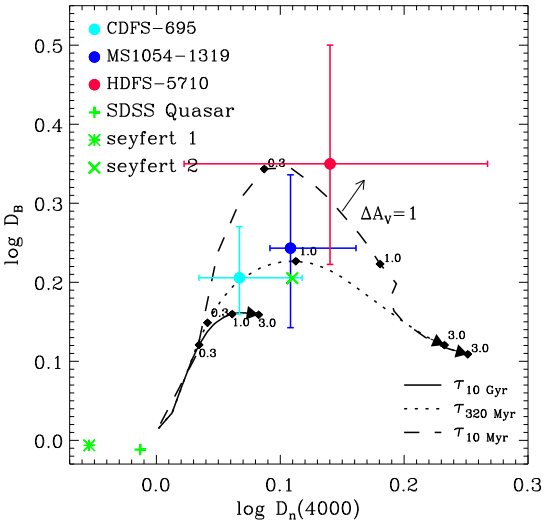

Fig. 5.— The Balmer break versus the 4000 Å break for the three studied galaxies and three different star-formation models. The small black diamonds and the corresponding values indicate the age in Gyr. The effect of attenuation is indicated as a vector in the plot. Measurements for three type of AGNs are shown as well (Francis et al. 1991). This figure illustrates that a dust-free $\tau_{10\mathrm{Gyr}}$ (which is comparable to constant star formation for galaxies at $z > 2$) is unable to produce large breaks within 3 Gyr. For MS1054-1319 the combined break implies a stellar population of about 1 Gyr, while for CDFS-695 we find a younger stellar population. The large Balmer break of HDFS-5710 suggests that this galaxy is in a post-starburst phase, and that $\tau_{10\mathrm{gyr}}$ or CSF is highly unlikely. The large breaks for MS1054-1319 and in particular HDFS-5710 imply that the optical spectrum is dominated by stellar light.

of 25 $M_\odot$/yr, derived from the 3σ upper limit on Hα and assuming the best-fit A_V of 0.9 mag. For MS1054-1319 $W_{H\alpha}$ provides additional evidence that the stellar light is dominated by evolved stars. And, in agreement with all the modeling results, CDFS-695 is still forming stars at a high rate.

We note that for CDFS-695 and MS1054-1319 there are indications that Hα is not entirely due to photo-ionization from star formation. The unusually high [NII]/Hα ratios could suggest that another source of ionization is contributing to $W_{H\alpha}$ (van Dokkum et al. 2004, 2005) of these two galaxies.

4.3. *Active Galactic Nuclei?*

Optical spectroscopy, X-ray studies, and 24μm imaging infer that about 5% to 25% of the DRGs show signs of AGN activity (Wuyts et al. in prep.; Rubin et al. 2004; Reddy et al. 2005; Papovich et al. 2006; Webb et al. 2006), depending on K-band depth of the sample and the type of AGN. AGNs affect rest-frame optical spectra in two ways; they contaminate the stellar continuum emission and produce characteristic emission line shapes and ratios. Continuum contribution from an AGN weakens the stellar break strength, and the strong breaks for HDFS-5710 and MS1054-1319 (see Fig. 5) imply that an AGN cannot be the dominant contributer to the rest-frame optical continua of these galaxies. For CDFS-695 the observed optical break is relatively weak and a sig-

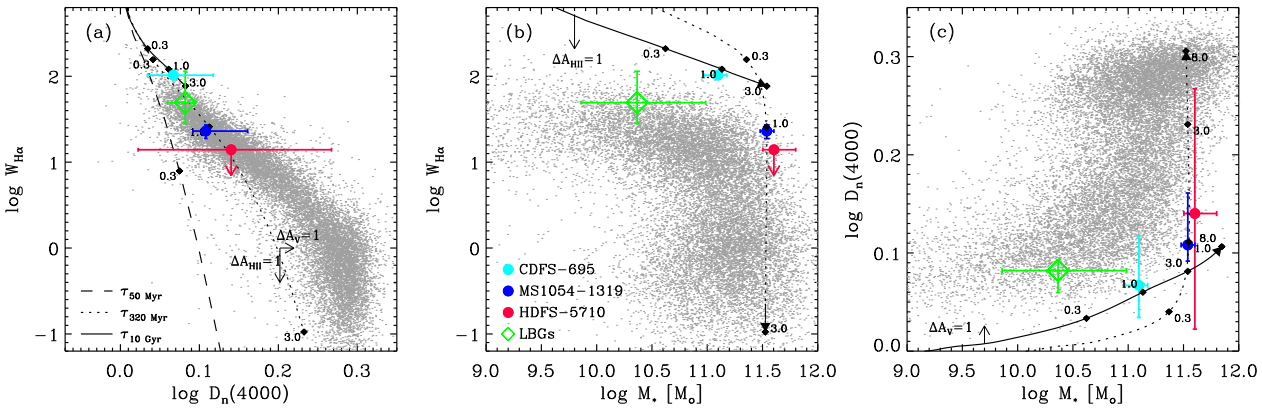

FIG. 6.— Comparison of spectral properties of the three studied galaxies with LBGs (*green*, Erb et al. 2003), and SDSS galaxies (*small grey dots*, Tremonti et al. 2004; Kauffmann et al. 2003a,b). Evolution tracks for $\tau_{10\rm Gyr}$ (*solid line*), $\tau_{320\,\rm Myr}$(*dotted line*) and $\tau_{50\rm Myr}$ (*dashed line*) models, derived from the Bruzual & Charlot (2003) library and the Kennicutt (1998) law are overplotted without correction for dust. The small black diamonds and the corresponding values indicate the age in Gyr. The correction for the integrated attenuation of the whole galaxy and extra extinction towards HII regions on the models are indicated by vectors. (a) $W_{H\alpha}$ versus $D_n(4000)$. (b) $W_{H\alpha}$ versus the stellar mass. (c) $D_n(4000)$ versus stellar mass. The masses of the galaxies are derived from the best-fit stellar model.

nificant AGN contribution to the continuum cannot be ruled out. We note that a minor nuclear contribution, as for a Seyfert 2 (Fig. 5), would imply that the stellar breaks are even stronger, which would yield older ages for the galaxies.

There is additional evidence that MS1054-1319 and CDFS-695 do not host an AGN which dominates the rest-frame optical continuum. NICMOS imaging of MS1054-1319 shows that the emission from this galaxy is extended (Toft et al. in prep). Furthermore, this galaxy is not detected in X-rays (Rubin et al. 2004) and there is no indication for an AGN in the rest-frame UV-spectrum (van Dokkum et al. 2003, ID 1671). For CDFS-695 the rest-frame UV spectrum lacks AGN features (Daddi et al. 2004a), although the unusual high [NII]/Hα ratios mentioned in the previous section could indicate an AGN contribution to this galaxy (van Dokkum et al. 2005).

5. COMPARISON TO OTHER GALAXIES

In the previous sections we learned through modeling and measuring the spectra that the DRG sample contains galaxies with a wide variety of properties. In this section we compare the measured and modeled properties with those of other high-z and low-z galaxy samples.

5.1. *Comparison to other high-redshift galaxies*

Several studies find that at similar rest-frame V magnitude and redshifts, DRGs are older, more massive, and dustier than LBGs (van Dokkum et al. 2004; Förster Schreiber et al. 2004; Labbé et al. 2005). We compare in this section the properties of the studied DRGs with those of LBGs at similar redshift, using the spectral indices and modeling results derived in previous sections. Ideally the samples should be matched in K band magnitudes or stellar masses. As such matched samples are not available caution is required when interpreting the differences.

As there are no optical break measurements of LBGs, we have to rely on the 'predicted' break, based on the best fitted SEDs. We used the BX and MD galaxies presented by Erb et al. (2003), which have a median redshift of $z \sim 2.3$. The photometry and best fit models of the galaxies are kindly provided by D.K. Erb; 4 galaxies of these are presented by Shapley et al. (2005). The break has been derived for each of the 12 galaxies in the Q1623 and Q1700 fields individually and yield a median $D_n(4000)$ of $1.21^{+0.03}_{-0.06}$. The $W_{H\alpha}$ for the BX/MD sample is derived from the $L_{H\alpha}$ presented by Erb et al. (2003) and the best fit models. These values are quite uncertain as slit-losses can introduce errors of up to about 50% in the absolute fluxes (Pettini et al. 2001). The predicted $D_n(4000)$ and $W_{H\alpha}$ of the BX/MD sample are plotted in Fig. 6a.

While our galaxies span different stages of stellar population evolution, the LBGs are located on the young and star forming part of the plot (Fig. 6a). Both DRGs and LBGs fall nicely on the predicted $\tau_{320\,\rm Myr}$ track.

The LBGs plotted here are all fainter than $K = 20$, and thus it could be that brighter LBGs have properties more similar to those of the plotted DRGs (Adelberger et al. 2005; Shapley et al. 2004). Also the difference in stellar mass of the LBGs and DRGs could be the cause of the different properties found for both samples. To show how both properties relate to stellar mass, we plotted $W_{H\alpha}$ and $D_n(4000)$ versus the stellar mass in Fig. 6b and 6c respectively. The DRGs MS1054-1319 and HDFS-5710 do not only have larger breaks and smaller $W_{H\alpha}$ than the BX/MD galaxies from Erb et al. (2003), but have also much higher stellar masses. As they span different ranges in stellar mass, it is difficult to directly compare the properties of the published samples, or interpret it in the context of evolutionary scenarios linking LBGs and DRGs.

5.2. *Comparison with low-z galaxies*

To examine the implications for the evolutionary histories of nearby galaxies we now compare the breaks, $W_{H\alpha}$, and masses of $z > 2$ galaxy populations with those of SDSS galaxies. The $D_n(4000)$ and $W_{H\alpha}$ (uncor-

rected for dust) of the SDSS galaxies are adopted from the catalogs presented in Kauffmann et al. (2003a) and Tremonti et al. (2004) respectively. We used the median dust-corrected stellar masses (Kauffmann et al. 2003a). Kauffmann et al. (2003a) used the same stellar library (Bruzual & Charlot 2003) to derive the stellar masses, but adopted the IMF by Kroupa (2001). At a given rest-frame V-band luminosity, the Kroupa (2001) IMF yields masses which are about a factor of 2 lower than the masses obtained using a Salpeter (1955) IMF between 0.1-100 $M_\odot$ (Bruzual & Charlot 2003), and we applied this correction to the SDSS galaxies.

In Fig. 6a the SDSS galaxies show a tight relation between $D_n(4000)$ and $W_{H\alpha}$. Remarkably, DRGs and LBG fall on this same low-redshift relation. The similarity of the $z \sim 2.3$ galaxies and SDSS galaxies breaks down when we include the stellar mass in Figs. 6b and c. At a given mass the $z \sim 2.3$ galaxies have on average smaller breaks and higher $W_{H\alpha}$ than the low-redshift galaxies. This implies that they are younger and have higher specific SFRs than their low-redshift analogs. Furthermore, galaxies with the properties observed for the $z \sim 2.3$ DRGs are rare at low redshift.

To show how simplified SFHs for HDFS-5710 and MS1054-1319 behave in this plot, we plotted the tracks for the $\tau_{320\,\mathrm{Myr}}$ and $\tau_{10\mathrm{Gyr}}$ models, scaled such that both models form the stellar mass of MS1054-1319 and HDFS-5710 within 3 Gyrs. A straightforward explanation for the location of DRGs on Fig. 6a–c is that they evolve into galaxies with properties comparable to those of the most massive and oldest galaxies in the SDSS. This may imply that the DRGs are the younger progenitors of galaxies of similar mass today.

6. SUMMARY AND CONCLUSIONS

We have presented rest-frame optical spectra of three DRGs at $z \sim 2.3$. To avoid a bias towards galaxies with strong UV emission, we selected objects which did not necessarily have a spectroscopic redshift from emission lines prior to the observations. We were able to measure the continuum shape and directly detect the Balmer/4000 Å break for all galaxies we observed for this purpose. This presents a significant advance beyond previous studies which were based on broadband photometry (e.g. Papovich et al. 2001; Shapley et al. 2001; Rudnick et al. 2003; Förster Schreiber et al. 2004; Papovich et al. 2006) or rest-frame optical emission lines (e.g. Erb et al. 2003; van Dokkum et al. 2004; Swinbank et al. 2004).

We have explored how the direct measurement of the optical continuum shapes and in particular the Balmer and 4000 Å break can contribute to our understanding of $z > 2$ galaxies. First, we have demonstrated that fairly accurate redshifts for red $z \sim 2.3$ galaxies can be obtained by modeling the rest-frame optical continuum around the Balmer/4000 Å break. The uncertainties on the modeled redshifts range from $\Delta z/(1+z) \sim 0.001 - 0.04$, depending on the S/N of the spectrum and the strength of the break. Our continuum redshifts agree very well with the emission line redshifts available for 2 of the 3 galaxies (within 0.5%). This opens up the possibility of deriving redshifts for UV-faint evolved galaxies, which are underrepresented in high redshift samples selected in optical surveys and are too faint for optical spectroscopy. Second, we used the rest-frame optical spectrum to study stellar populations and dust properties of galaxies, by modeling the spectrum and using spectral diagnostics. Spectral modeling is very effective in narrowing the range of possible solutions for age, star formation timescale and dust content. Including NIR spectra in photometric modeling leads to more tightly constrained properties of stellar populations in high redshift galaxies than modeling solely the optical-to-NIR photometry. And third, the break allows us to constrain the contribution from a possible AGN. In summary, studying the rest-frame optical shape appears to be crucial for understanding the red $z > 2$ galaxy population, and provides information which is difficult – and in some cases impossible – to obtain by other means.

The spectral modeling presented here for the three galaxies confirms the large variation among the SED properties and SFHs of DRGs (e.g. Förster Schreiber et al. 2004; Labbé et al. 2005; Webb et al. 2006), as our objects range from a dusty starburst with a small break to an apparently evolved galaxy with a strong 4000 Å break and no detected Hα emission. For the galaxy without emission lines, we derived the redshift from the spectral continuum shape. The stellar masses of the two most evolved galaxies (age $\sim$ 1.3-1.4 Gyr) are about $4 \times 10^{11} M_\odot$, and thus they are among the most massive galaxies yet identified at these redshifts. Comparison to low redshift galaxies suggest that they probably evolve into galaxies with properties comparable to those of the most massive and oldest galaxies in the low-redshift Universe. The younger starburst galaxy (0.3 Gyr) has a stellar mass of $1 \times 10^{11} M_\odot$. The strong breaks in the two most evolved galaxies imply that stellar light is the dominant contributor to the optical emission. For the younger galaxy a significant contribution from an AGN cannot be ruled out.

The next step to increase our understanding of high-redshift galaxy populations is to extend our NIR spectroscopic sample. The present sample does not allow any statistical analysis, and is mainly an illustration of the capabilities NIR spectroscopy has to offer. A larger sample will tell us more about the ratio of evolved versus star-forming $z > 2$ galaxies, and the contribution of AGNs.

This research would have been impossible without the generosity and flexibility of the staff of the Gemini Observatory. We are grateful to the referee for very useful comments, that greatly improved the paper. We thank Dawn Erb for providing the photometry and model parameters of the BX/MD sample. This research was supported by grants from the Netherlands Foundation for Research (NWO), and the Leids Kerkhoven-Bosscha Fonds. Support from National Science Foundation grant NSF CAREER AST-0449678 is gratefully acknowledged. DM is supported by NASA LTSA NNG04GE12G. EG is supported by the National Science Foundation under Grant No. AST-0201667, an NSF Astronomy and Astrophysics Postdoctoral Fellowship (AAPF). ST acknowledges the support of the Danish Natural Research Council. The Keck Observatory was made possible by the generous financial support of the W.M. Keck Foundation. The

authors wish to recognize and acknowledge the very significant cultural role and reverence that the summit of Mauna Kea has always had within the indigenous Hawaiian community. We are most fortunate to have the opportunity to conduct observations from this mountain.

REFERENCES

Adelberger, K.L., Steidel, C.C., Pettini, M., Shapley, A.E., Reddy, N.A., & Erb, D.K. 2005, ApJ, 620, L75
Balogh, M.L., Morris, S.L., Yee, H.K.C., Carlberg, R.G., & Ellingson, E. 1999, ApJ, 527, 54
Beers, T.C., Flynn, K., & Gebhardt, K. 1990, AJ, 100, 32
Bruzual A.G., 1983, ApJ, 273, 105
Bruzual, G. & Charlot, S. 2003, MNRAS, 344, 1000
Calzetti, D., Armus, L., Bohlin, R.C., Kinney, A.L., Koornheef, J., & Storchi-Bergmann, T. 2000, ApJ, 533, 682
Daddi, E. et al. 2004b, ApJ, 600, L127
Erb, D.K., et al. 2003, ApJ, 591, 101
Förster Schreiber, N.M. et al. 2004, ApJ, 616, 40
Förster Schreiber, N.M. et al. 2006, AJ, in press (astro-ph/0510186)
Francis, P.J., Hewett, P.C., Foltz, C.B., Chaffee, F.H., Weymann, R.J., & Morris, S.L. 1991, ApJ, 373, 465.
Franx, M. et al. 2003, ApJ, 587, L79
Gawiser, E. et al. 2005, ApJS, 162, 1
Giavalisco, M. et al. 2004 ApJ, 600, L93
Hamilton, D. 1985, ApJ, 297, 371
Kauffmann, G. et al. 2003a, MNRAS, 341, 33
Kauffmann, G. et al. 2003b, MNRAS, 341, 54
Kennicutt, R.C. 1998, ARA&A, 36, 189
Kroupa, P. 2001, MNRAS, 322, 231
Labbé, I. et al. 2005, ApJ, 624, L81
Madau, P., Ferguson, H.C., Dickinson, M.E., Giavalisco, M., Steidel, C.C., & Fruchter, A. 1996, MNRAS, 283, 1388
McLean, I. S., et al. 1998, Proc. SPIE, 3354, 566
Papovich, C., Dickinson, M., & Ferguson, H.C. 2001, ApJ, 559, 620
Papovich, C., et al. 2006, ApJ, in press (astro-ph/0511289)
Pettini, M., Shapley, A.E., Steidel, C.C., Cuby, J.-G., Dickinson, M., Moorwood, A.F.M., Adelberger, K.L., & Giavalisco, M. 2001, ApJ, 554, 981
Reddy, N.A., Erb, D.K., Steidel, C.C., Shapley, A.E., Adelberger, K.L., & Pettini, M. 2005, ApJ, 633, 748
Rubin, K.H.R., van Dokkum, P.G., Coppi, P., Johnson, O., Förster Schreiber, N.M., Franx, M., & van der Werf, P. 2004, ApJ, 613, L5
Rudnick, G., et al. 2001, AJ, 122, 2205
Rudnick, G., et al. 2003, ApJ, 599, 847
Salpeter, E.E. 1955, ApJ, 121, 161
Sawicki, M., & Yee, H.K.C 1998, AJ, 115, 1329.
Shapley, A.E, et al. 2005, ApJ, 626, 698
Shapley, A.E., Erb, D.K., Pettini, M., Steidel, C.C., & Adelberger, K.L. 2004 ApJ, 612, 108
Shapley, A.E., Steidel, C.C., Adelberger, K.L., Dickinson, M., Giavalisco, M., & Pettini, M. 2001, ApJ, 562, 95
Simpson, C., Dunlop, J.S., Eales, S.A., Ivison, R.J., Scott, S.E., Lilly, S.J., & Webb, T.M.A. 2004, MNRAS, 353, 179
Steidel, C.C., Giavalisco, M., Pettini, M., Dickinson, M., & Adelberger, K.L. 1996a, ApJ, 462, L17
Steidel, C.C., Giavalisco, M., Dickinson, M., & Adelberger, K.L. 1996b, AJ, 112, 352
Steidel, C.C., Adelberger, K.L., Shapley, A.E., Pettini, M., Dickinson, M., & Giavalisco, M. 2003, ApJ, 592, 728
Swinbank, A. M., Smail, I., Chapman, S., Blain, A.W., Ivison, R.J., & Keel, W.C. 2004, ApJ, 617, 64
Tremonti, C.A. et al. 2004, ApJ, 613, 898
Vanzella, E. et al. 2005, A&A, 434, 53
van Dokkum, P.G. 2001, PASP, 113, 1420
van Dokkum, P.G. et al. 2003, ApJ, 587, L83
van Dokkum, P.G. et al. 2004, ApJ, 611, 703
van Dokkum, P.G., Kriek, M., Rodgers, B., Franx, M., & Puxley, P. 2005, ApJ, 622, L13
van Dokkum, P.G., et al. 2006, ApJ, 638, L59
Webb, T.M.A., et al. 2006, ApJ, 636, L17